Granular Clustering Studied in Microgravity

Meiying Hou, Wenguang Wang and Qian Jiang

Abstract Energy dissipation is one of the most important characteristics of granular gas, which makes its behavior different from that of molecular gas. In this chapter we first show the investigations on the freely-cooling evolution of granular gas under microgravity in a drop tower experiment, the granular segregation in a two-compartment cell, known as Maxwell's Demon phenomenon in granular gas, is then shown, which is investigated in SJ-10 satellite. DEM simulations of both investigations are given. The simulation results on granular freely-cooling evolution support Haff's law that the kinetic energy dissipates with time t as $E(t) \sim (1 + t/\tau)^{-2}$, with a modified τ, of which the friction dissipation during collisions has to be taken into account. The DEM simulation on Maxwell's Demon with and without gravity shows that the segregation quantified by parameter is non-zero in zero gravity. However, not like the case with gravity, it does not depend on the excitation strength. The waiting time τ, in zero gravity, depends strongly on: higher the, lower the waiting time. The simulation results are confirmed by the SJ-10 satellite microgravity experiments. The major content of this chapter is adopted from our previous papers (Wang et al. Chin Phys B 26:044501, 2017 [1]; Chin Phys B 27:084501, 2018 [2]).

Keywords Granular gas · Clustering · Freely cooling · DEM simulation · Microgravity · Segregation

1 Freely-Cooling Evolution of Granular Gas

Granular gas is a dilute ensemble of grains interacting by dissipative collisions. This dissipative nature of particle interactions determines its ensemble properties, and distinguishes it from molecular gas. Most prominent feature is granular cooling that system loses kinetic energy permanently, with no external energy input. From a

M. Hou (✉) · W. Wang · Q. Jiang
Key Laboratory of Soft Matter Physics, Beijing National Laboratory
for Condensed Matter Physics, Institute of Physics, Beijing 100190, China
e-mail: mayhou@iphy.ac.cn

homogeneous excited-state, the system enters into an initial period of homogeneous energy loss, and later grains can spontaneously cluster [3–19]. Theoretical modeling [20–31] and simulation investigations [22–24, 26, 30, 32–41] are based on simplifications and assumptions of grain properties. Quantitative experiments are very much needed for better understanding of fundamental features of such ensembles [42–45]. In this section our investigations on the freely-cooling evolution of granular gas under microgravity in a drop tower experiment are given, and the molecular dynamics (MD) simulation is conducted for comparison [2].

In order to investigate the energy loss due to grain-grain collisions in steady excitation and during freely cooling, experiments need to counter balance the gravitational force to float the particles [16, 42]. In 2008, Maaß et al. used magnetic forces to make the granular particles float in a container [42]. In their experiment, diamagnetic particles were chosen. The total energy of a particle in a magnetic field B is $U = -\chi V B^2/2\mu_0 + mgz$ [46], where U is the potential energy of the particle, χ is the magnetic susceptibility, V is the volume of the particle, μ_0 is vacuum permeability, m is the mass of particle, g is the gravity, and z is the position of particle in the z direction. Since $\mathbf{F} = -\nabla U$ and the force balance requires $\mathbf{F} = 0$, $-\nabla U = -mg\mathbf{e}_z + \chi V \mathbf{B}\nabla\mathbf{B}/\mu_0 = 0$ and $\mathbf{B}\nabla\mathbf{B} = \mu_0\rho g/\chi$, where $\rho = m/V$ is the density of particle. Since $\nabla^2 U = -\chi V \nabla^2 \mathbf{B}^2/2\mu_0$ and $\nabla^2 \mathbf{B}^2 > 0$, for diamagnetic particles $\chi < 0$, $\nabla^2 U > 0$, therefore the diamagnetic particles can float stably in such an external magnetic field. Maaß et al. used this method to make the particles float. They have successfully observed two stages. At early time, the evolution of the kinetic energy dissipation of granular gas follows Haff's law. At a later time, the granular gas clusters and behaves like a single particle motion, which depends on the size of the container.

Tatsumi et al. reported in 2009 the first microgravity experimental investigations on freely cooling granular gas system. Their microgravity experiment was performed during parabolic flight. They studied the kinetics of both freely cooling and steadily driven granular gas system in quasi-two-dimensional cells under micro-gravity [43]. Due to the g-jitter of the parabolic flights, Tatsumi et al. could observe only within one second of the cooling process. Their granular temperature decays as $T_g = T_0(1 + t/\tau)^{-2}$, which is consistent with the Haff's law that $E(t) \sim (1 + t)^{-2}$.

Very recently Kirsten Harth et al. studied freely cooling of a granular gas of rod-like particles in microgravity. For rod-like particles they found that the law of $E(t) \sim t^{-2}$ is still robust [45]. A slight predominance of translational motions, as well as a preferred rod alignment in flight direction were also found.

These studies concerned the form of kinetic energy dissipation with time. Recently, a Drop Tower micro-gravity experiment was conducted and the results were compared with simulations. Some detailed factors (such as restitution coefficient, number density, particles size) which affect Haff's law were shown. Taking into consideration the collision friction, the characteristic decay time τ in the model is modified. Experimental and simulation results show that the average speed of all particles in granular gas decays with time t as $v \sim (1 + t/\tau)^{-1}$ and the kinetic energy decays with time t as $E(t) \sim (1 + t/\tau)^{-2}$ as predicted in Haff's law. However, the clustering mode, as reported in Maaß's et al. work [42], was not observed in this recent work [2] due to its short (5 s) cooling observation time.

1.1 Haff's Freely Cooling Model

Haff's theory about freely cooling granular is based on the classical thermodynamics [20, 21]. There are several assumptions to simplify the analysis of freely cooling process of dilute granular gas. Firstly, the restitution coefficient is constant for each collision among particles. Secondly, the granular gas system must be homogeneous, so the mean free path is meaningful in the analysis and can be used to calculate the collision frequency. Thirdly, only collisions among particles contribute to the energy dissipation in the theory, while the part due to friction is not taken into account. Fourthly, the size of particles is relatively small compared with the mean free path.

The mean free path of particles in dilute and homogeneous granular gas is $\lambda = 1/(n\sigma)$, where n is the number density and $\sigma = \pi(2R)^2$ is the cross section of particles respectively. Here R is the particles' radius. The kinetic energy E of one-unit volume of granular gas is proportional to $nm\bar{v}^2/2$, namely $E \propto nm\bar{v}^2/2$, where $\bar{v}$ is the average speed of particles. When a particle collides with another one, the average kinetic energy loss of a particle is proportional to $(1 - e^2)m\bar{v}^2/2$. The collision frequency of a single particle, is $\bar{v}/\lambda$. The collision frequency of whole system will be $n\bar{v}/\lambda$. But a single collision between two particles is counted twice in a whole system, the actual collision frequency of the system is $n\bar{v}/2\lambda$. The total kinetic energy loss per unit time of one-unit volume of granular gas is

$$\Delta E = -\frac{(1 - e^2)nm\bar{v}^3}{4\lambda}. \tag{1}$$

The change of kinetic energy per unit time equals the loss of the energy per unit time due to collisions between particles,

$$\frac{d}{dt}\left(\frac{1}{2}nm\bar{v}^2\right) = -(1 - e^2)\frac{nm\bar{v}^3}{4\lambda}. \tag{2}$$

The solution of Eq. (2) gives

$$\bar{v}(t) = \frac{\bar{v}_0}{1 + t/\tau}, \tag{3}$$

$$\tau = \frac{4}{(1 - e^2)\bar{v}_0 n\sigma}, \tag{4}$$

where $\bar{v}_0$ is the initial average speed of the granular particles. We notice that Eq. (4) is different from that used in Maaß's research [42] by a factor of 2. Our simulation results support Eq. (4).

The kinetic energy E is proportional to $\bar{v}^2$, the evolution of kinetic energy, thus, is

$$E = \frac{E_0}{(1 + t/\tau)^2}. \tag{5}$$

After a duration of τ since the granular gas begins to cool freely, the average velocity of the system will drop by half as given in Eq. (3). This parameter has also been used in Brilliantov and Pöschel's paper [31, 43] that is,

$$\tau^{-1} = 2\sqrt{\frac{T_0}{\pi}}\left(1 - e^2\right)\frac{1 - (7/16)\phi}{(1 - \phi)^2}\frac{\phi}{d},\tag{6}$$

where T_0 is the initial granular temperature, d is the diameter of particle, and ϕ is the volume friction. In order to compare with their work, we also study the dependence of characteristic decay time τ on material parameters (the restitution coefficient e and the particle size R), and also the initial velocity of the system, $\bar{v}_0$. The τ dependence shows the complex property of granular matter—the historical dependency.

Most previous researches mainly concerned the form of Eq. (3), and the exact expression of τ is not yet unique. Hence, we pay more attention to the characteristic decay time τ here, and our numerical results support the form of Eq. (4).

1.2 Experiment

To study the granular gas cooling behavior on ground, gravity has to be counteracted by an external force, like buoyancy in liquid, electric or magnetic field force. For example, Maaß et al. used magnetic gradient to make the diamagnetic particle float [42]. Soichi Tatsumi et al. were the first to attempt microgravity experiment studying the freely cooling granular gas behavior in the parabolic flights [43]. However, due to the g-jitter during the flights, their cooling observations were no longer than 1.6 s. In the present work, we achieve microgravity in Bremen Drop Tower. The Bremen Drop Tower, with a height of 146 m, providesup to 10^{-6} g microgravity condition with a duration as long as 9.3 s.

In the experiments, the catapult operation mode with a weightless duration of 9.3 s was adopted. By this means, a drop capsule Fig. 1a, b was thrown from the bottom of the tower to the top and back into a buffer container filled with foam pellets. Before the freely cooling phenomenon is observed, the particles had to move at a certain initial velocity. In the initial 3 or 4 s, the granular gases were driven by two pistons which were controlled by two linear motors separately Fig. 1c. Then the motor was powered off, the process of freely cooling started. A high-speed camera was used to process and analyze the particle trajectories.

The size of the sample cell is $150 \times 50 \times 10$ mm. Three sub cells are separated by two pistons as is shown in Fig. 2. The numbers of particles in each subcell from left to right in Fig. 2 are 171, 286 and 64, respectively. The diameters of particles in each subcell from left to right are 2.5 mm, 2 mm and 2.5 mm, respectively. Particle motions are initiated by the two pistons, whose central positions, vibration frequencies and amplitudes are controlled. The pistons are stopped after 3–4 s for the fast camera to take images of grain motion during cooling. The image data in the middle and the right subcell are processed and analyzed. Two drop experiments are conducted. The key parameters in each experiment can be found in Table 1 of reference [2].
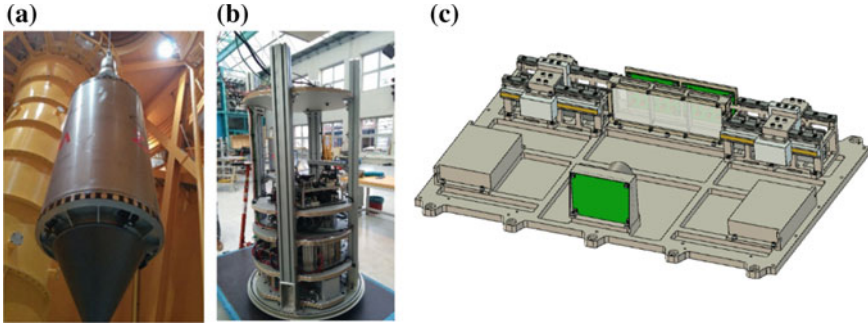
Fig. 1 **a** The drop capsule; **b** Inside the capsule: power system and experimental device; **c** Sketch of the experimental module
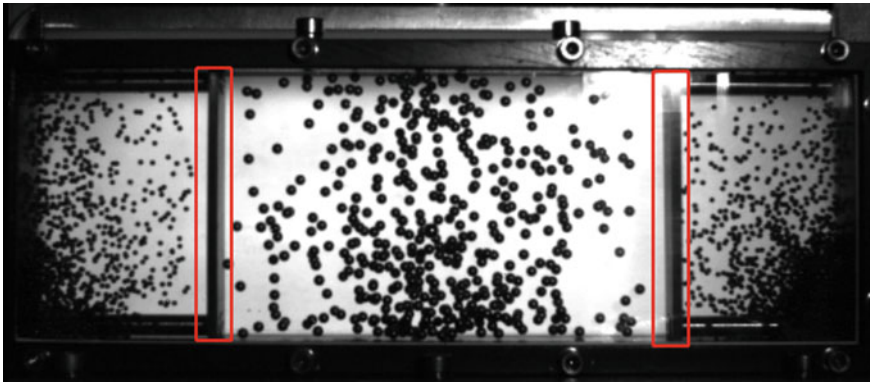

Fig. 2 Sample cell where two pistons are marked by red lines

1.3 Experimental Results

The experimental images are captured by a high-speed camera of 500 fps. Each frame of the image is of 512×512 pixels. The resolution of experimental images is about 0.3 mm/pixel, therefore the particle sizes with diameters 2 and 2.5 mm are about 6–7 pixels and 8–9 pixels, respectively. However, since we have only one camera, we can observe only a two-dimensional projection of the particle three-dimensional motion. Some trajectories of two overlapped particles may not be identified. Over exposure in one of the cell corners also hinders tracing particles in that area. Despite of all these, we can trace more than 95% of the total particles.

Figure 3a shows the trajectories of all the traceable particles in the freely cooling processes. Not all the particles can be traced at all times. The average end speeds of particles in these four sets of experiments are about 4–5 mm/s. The average speed decreases by an order of magnitude in 4–5 s. Figure 3b shows that many particles move in a local area before they cool down.
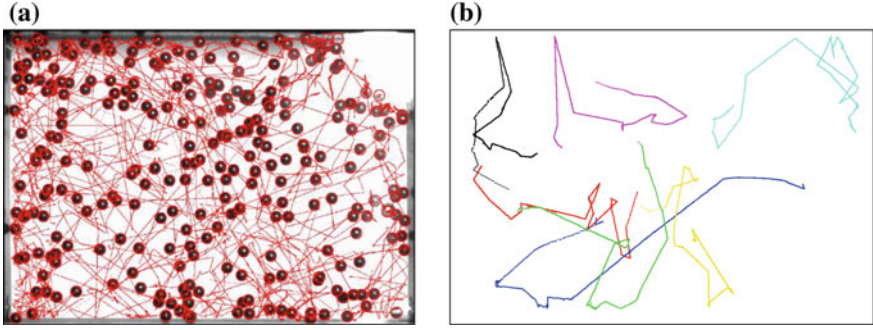
Fig. 3 **a** Traces of all particles in freely cooling process; **b** Demo of few traces of particles (adapted from Wang et al. [2])
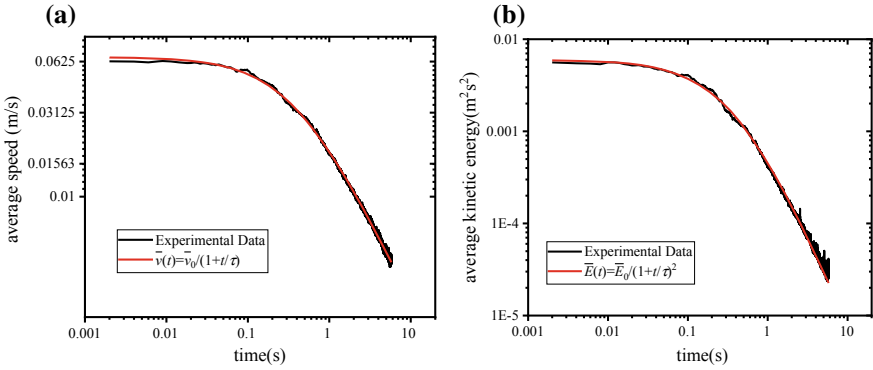

Fig. 4 **a** Average speed and **b** average kinetic energy of particles as a function of time (adapted from Wang et al. [2])

The speed of each particle v_i is calculated from $v_i = \sqrt{v_{ix}^2 + v_{iy}^2}$, where v_{ix} is the ith particle velocity along the excitation direction, and v_{iy} is the velocity of the particle along the perpendicular y direction. The $\bar{v}$ denotes the average velocity of all particles. Here we set the mass of a particle $m = 1$, so the average kinetic energy is $\bar{E} = <v_i^2>$. In Fig. 4 we fit the average speed and the average kinetic energy of particles by Haff's law. It is seen that Haff's equation fits well, although it does not take into consideration the inelastic collisions with the rigid walls nor frictions in the particle-particle collisions. The values of the two fitting parameters in Haff's law $\bar{v}_0/(1 + t/\tau)$, i.e., $\bar{v}_0$ (the initial average speed) and τ (the decay time), in the four sets of experiments are given in Table 2 of reference [2].

In our experiments, collisions with the two pistons provide particles with initial velocities in the x direction. Figure 5 shows time evolutions of both $\bar{v}_x$ and $\bar{v}_y$, which are consistent with those from the Haff's law. Since particles gain velocities in the y
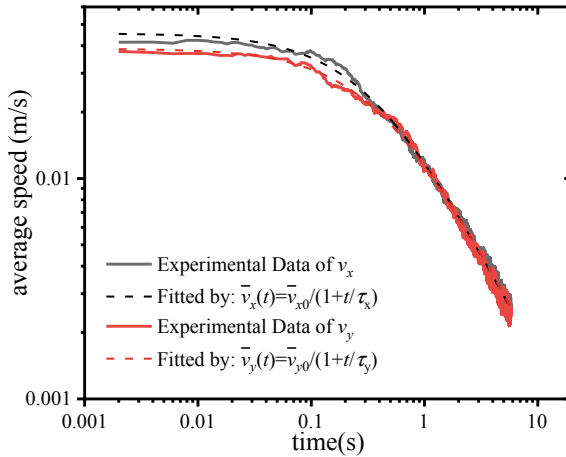
Fig. 5 Average speeds in vertical (x, black curves) direction and horizontal (y, red curves) direction decaying with time (adapted from Wang et al. [2])

direction through particle-particle collisions, the initial $\bar{v}_y$ is seen to be smaller than that of $\bar{v}_x$ due to the dissipation caused by the inelastic collisions. However, we see in Fig. 5 that although initially $\bar{v}_x$ is greater than $\bar{v}_y$, it takes about the same time (approximately 0.5 s) for them to reduce to the same velocity. This again is predicted by Haff's Law. As we can see, when the time t is large enough compared with the characteristic decay time τ, Eq. (3) becomes

$$\bar{v}(t) \cong \frac{\bar{v}_0}{t/\tau}. \tag{7}$$

Substituting Eq. (4) into Eq. (7), we have

$$\bar{v}(t) = \frac{4}{\left(1 - e^2\right)n\sigma t}. \tag{8}$$

Equation (8) shows that when $t \gg \tau$, the average speeds do not depend on the initial velocities, and the velocities of different directions converge into the same value. The average velocity depends on the restitution coefficient and the particle number density.

The kinetic energy E is proportional to the square of the average speed of particles $\bar{v}^2$. The kinetic energy of each dimension in freely cooling state obeys the energy equipartition theorem.

1.4 Simulation Results

Considering the limitation of the experimental opportunities, we perform simulations based on discrete elements method (DEM) [1, 47]. The cell size in the simulation is fixed at $10 \times 10 \times 10$ cm. In Haff's theory, the contribution of the energy dissipation caused by friction during collision between particles is not considered. But in reality, friction exists. In this simulation, the influence of friction is considered.

Figure 6 shows the decays of the simulated average speed with and without considering friction. It is seen that it decays faster when friction is considered. Both can be fitted to Haff's law, but with different values of τ. Haff's freely cooling law is rather robust even though several assumptions in the theory are not satisfied. In the following section, the influence of friction on τ will be discussed.

1.4.1 Effects of Restitution Coefficient and Friction on Characteristic Time τ

Figure 7 shows the simulation results for the τ versus restitution coefficient e when friction is not taken into account. Green line is plotted by using Eq. (4). The inset in Fig. 7 shows the linear relationship between τ and $(1-e^2)^{-1}$. When the restitution coefficient e is close to 1, the τ approaches to infinity.

Figure 8 shows the simulated τ versus restitution coefficient e with taking rotation and friction into account. The inset of Fig. 8 still shows the good linear dependence of τ on $(1-e^2)^{-1}$, however, the intersection shifts. We consider the shift to be due to rotation and friction by adding a γ term $(1-e^2 + \gamma)^{-1}$. The total kinetic energy loss after each collision on average is $\Delta E = (1-e^2 + \gamma)E$. Equation (4) is thus modified into

Fig. 6 Average speeds decaying with time t with (blue dot) and without (green dot) considering friction (adapted from Wang et al. [2])
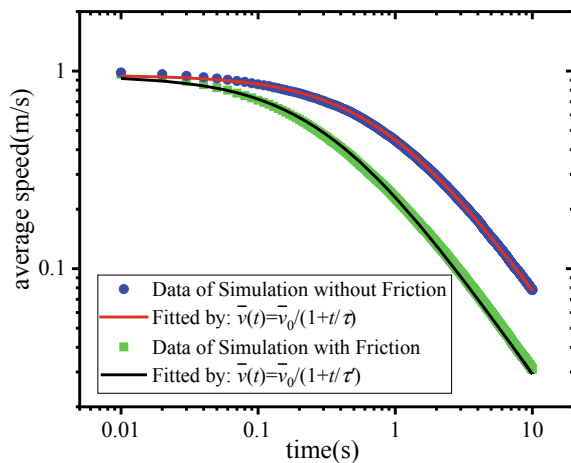
Fig. 7 Simulated τ versus the restitution coefficient e with no friction. Inset shows linear relationship between $(1-e^2)^{-1}$ (adapted from Wang et al. [2])
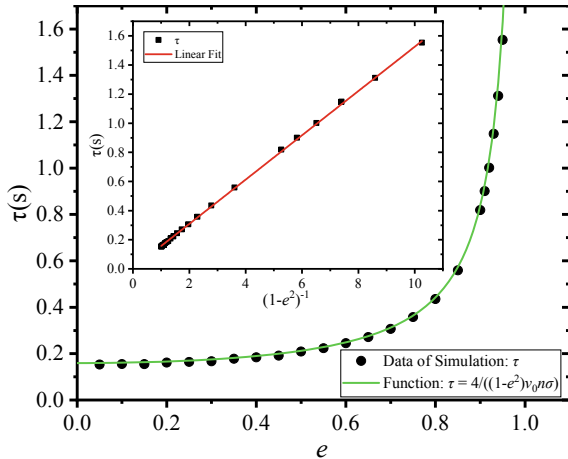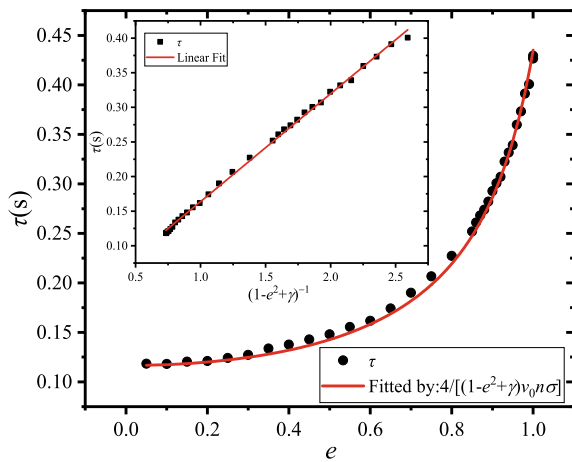

Fig. 8 Simulated τ versus restitution coefficient e with friction. Inset shows linear relationship between $(1-e^2 + \gamma)^{-1}$ and τ (adapted from Wang et al. [2])

$$\tau = \frac{4}{\left(1 - e^2 + \gamma\right)\bar{v}_0 n\sigma}. \tag{9}$$

The red curve in Fig. 8 is fitted by Eq. (9), and the inset figure shows a good linear relationship between τ and $(1-e^2 + \gamma)^{-1}$. The friction coefficient in this group of simulations is taken to be 0.3, and the corrective frictional term γ fitted by Eq. (9) equals 0.37. Figure 9 shows that the $(1-e^{-2}) \sim 1/\tau$ straight lines with friction and without friction are almost parallel. The difference between the intercepts with x-axis of the two lines is 0.38, which is very close to the fitted value 0.37. The above result indicates that our assumption and modification are reasonably good when the influence of friction during the collision among particles is considered.
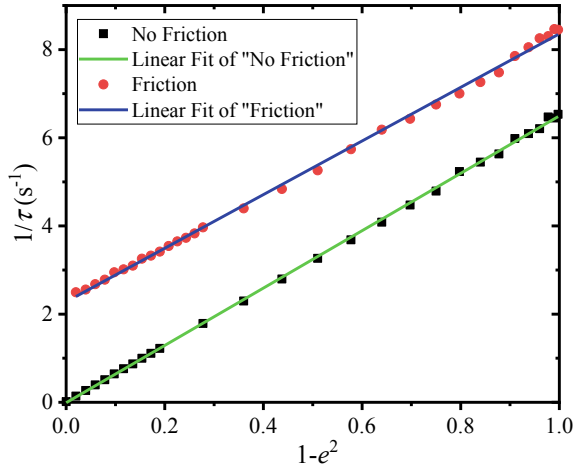
Fig. 9 Plots of $(1-e^{-2}) \sim 1/\tau$ are both straight lines with and without considering friction. Straight line (blue) with considering friction shifts upward with respect to straight line (green) without considering friction (adapted from Wang et al. [2])

1.4.2 Effects of Number Density and Particle Size on Characteristic Decay Time τ

From Eq. (4), it can be seen that $1/n$ and $1/R^2$ have a linear relationship with τ respectively. The inset in Fig. 10 shows that the effect of the number density on τ obeys Haff's law while other parameters hold constant, $e = 0.8$, $R = 1$ mm. The inset in Fig. 11 shows that the effect of the size of particles on τ nearly follows Eq. (4), but not strictly, while other parameters hold constant, $e = 0.8$ and $n = 2$ cm^{-3}. We notice that the slope of the curve in the inset becomes upward gradually. This means that the τ will be shorter with a larger size of particles. We recall that an assumption in Haff's law is that the size of particles must be relatively small compared with the mean free path λ of the granular gas system. Actually, when the size of particles is relatively large compared with λ, we must take into account the size of particles. The collision frequency is accurately related to the average separation s between neighboring particles, which depends on a surface-to-surface distance. A corrective term r_c must be subtracted from the mean free path λ to obtain an average separation s, namely $s = \lambda - r_c$. The corrective term is close to $1.654R$ according to Opsomer's work [48]. The collision frequency Z is calculated from $Z = \bar{u}/s = \bar{u}/(\lambda - 1.654R)$, where $\bar{u}$ is the average relative velocity during collisions among particles. The corrective term will contribute more to the collision frequency when the size of particles turns larger. Hence, the curve $1/\tau \sim R^2$ is a little concave as shown in the inset of Fig. 11.

Fig. 10 Decay time τ as a function of number density n. The inset shows linear relationship between n and $1/\tau$ (adapted from Wang et al. [2])
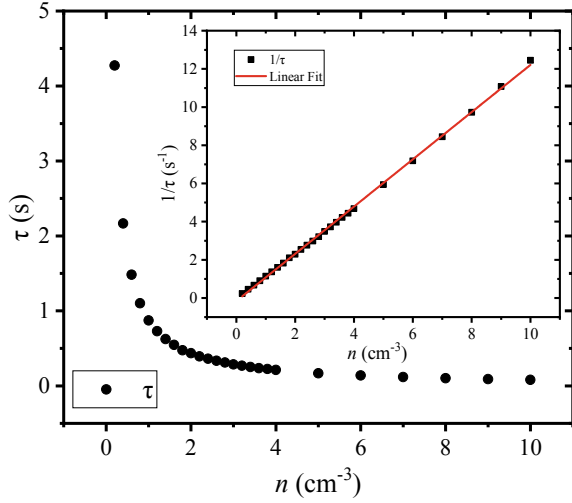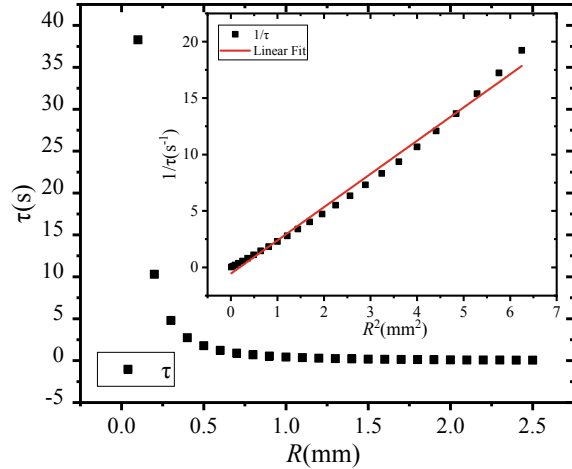

Fig. 11 Decay time τ as a function of particle radius R. Inset shows $R^2 \sim 1/\tau$ curve slopes upward gradually with respect to linear fitted line (adapted from Wang et al. [2])

1.4.3 Evolution of Velocity Distribution with Time

For a conservative classical ideal gas system in equilibrium state, the velocity distribution of each dimension follows the normal distribution. But it is still not widely accepted that what law the velocity distribution of a dissipative system like granular gas obeys. Figure 12a shows that our numerical simulation results of the velocity distribution at different times during the freely cooling obey their corresponding normal distribution. The scalar speed of each particle is set to be 1 m/s at the initial time, but the direction of velocity is randomly set. Although the velocity distribution does not satisfy the normal distribution at the initial time, it evolves into the normal distribution after a while. The standard deviation w represents the width of
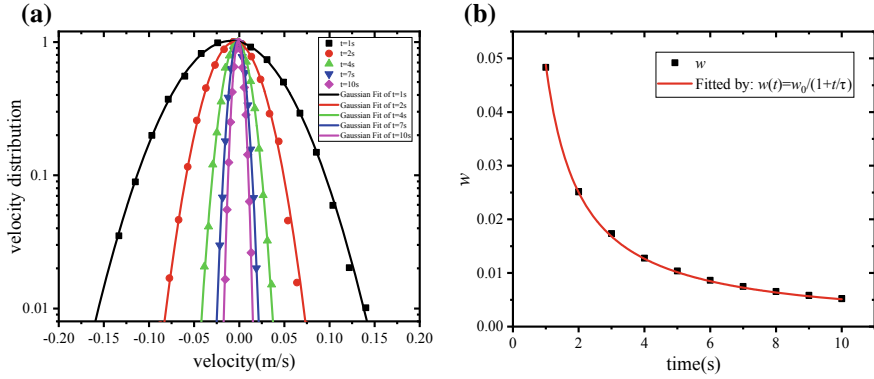
(a)

(b)

Fig. 12 **a** Evolutions of velocity distribution in one dimension with time. The number of particles is 10,000. The velocity distribution is standardized. **b** Standard deviation w of the normal distribution varying with time (adapted from Wang et al. [2])

the normal distribution curve. The width is related to the fluctuation of the average speed of particles and is defined as granular temperature. It is verified in Fig. 12b that standard deviation w evolving with time t obeys $w \sim (1 + t/\tau)^{-1}$ similar to the average speed of particles.

We recall that the state of energy equipartitions for freely cooling granular gas will be reached even if the symmetry is broken at initial time. Our numerical results show that the freely cooling granular gas not only follows Haff's law but also has two intrinsic properties, namely the energy equipartition and the normal velocity distribution.

2 Maxwell's Demon in Zero Gravity

Granular materials' extremely rich dynamical behaviors have attracted attention of physicists of different fields in recent years [3–5]. Examples are the heap formation of a granular bed [49–51] and the size segregation of a granular system with grains of various sizes under vertical vibration known as the Brazil Nut effects [52, 53]. In these phenomena, energy is being injected continuously into the system by the oscillating boundaries and propagated into the bulk by the inelastic collisions of the grains. A steady state of the whole system is reached when the dissipation of the system is balanced by the input of the energy. Since both the energy input and dissipation depend crucially on the configurations of the system, many intriguing steady states and even oscillatory states can be created.

Borrowing concepts from molecular gas system, low density granular system can be treated as a granular gas. The granular gas systems reach a steady state when input and loss of energy are balanced. They are not in thermal equilibrium and the laws of

thermodynamics for molecular gases do not apply to these systems. For example, the thermodynamically impossible phenomenon such as the Maxwell's demon [54, 55] has been observed and successfully explained. In such an experiment, granular gas confined in a compartmentalized system can be induced to segregate into one of the compartments by lowering the vibration amplitude of the system. In this latter case, a decrease of the configurational entropy of the system takes place spontaneously; as if the second law of thermodynamics is violated. In fact, other similar intriguing segregation [56] and ratchet effects [57] have also been reported in compartmentalized granular gases.

Granular Maxwell's Demon phenomenon has been studied in simulation [58–68], theoretical modeling [69–74], and by experiments [75–85] in recent years extensively. The segregation phenomenon relies on the existence of a non-monotonic flux, which determines the number of particles per unit time flows between the two compartments [55]. The flux function is derived from the equation of gas state and therefore depends on the gravity. If applicable, the phenomenon can be used to transport granular materials in space [86, 87]. In this section, simulation study is given to find the condition for possible segregation in two-compartment granular gas system in an environment of zero gravity.

2.1 Model

The simulation is based on discrete element method, in which each particle is treated as a discrete element [88, 89]. The motion of each particle obeys the Newton's Second Law. The interaction between them is considered if and only if two particles collide. Taking the rotation into consideration, the particles' equations of motion are as follows:

$$m_i \ddot{\vec{r}}_i = \sum_{j, j \neq i} \vec{F}_{ij}^C + \vec{F}_i^O, \tag{10}$$

$$I_i \dot{\vec{\omega}}_i = \sum_{j, j \neq i} \vec{R}_i \times \vec{F}_{ij}^C + \vec{M}_i^O, \tag{11}$$

where m_i, I_i, $\vec{r}_i$ and $\vec{\omega}_i$ are the mass, the moment of inertia, the displacement and the angular velocity of particle i, respectively. $\vec{F}_{ij}^C$ is the contact force that the particle i is applied by the particle j. $\vec{R}_i$ is the radius vector of particle i. $\vec{F}_i^O$ and $\vec{M}_i^O$ are other forces and torques applied to the particle i, such as the gravity force. Generally, $\vec{F}_{ij}^C$ can be decomposed into two parts: a normal component and a tangential one,

$$\vec{F}_{ij}^C = \vec{F}_{ij}^n + \vec{F}_{ij}^t. \tag{12}$$

The normal and the tangential contact forces between two particles are handled separately.

Two particles interact with each other only during contact. The overlap in the normal direction between particles i and j with radii R_i and R_j, respectively, is

$$\delta = (R_i + R_j) - (\vec{r}_i - \vec{r}_j) \cdot \vec{n}, \tag{13}$$

where δ is a positive number when the two particles interact, $\vec{n}$ is the unit vector of the relative displacement $\vec{n} = (\vec{r}_i - \vec{r}_j)/|\vec{r}_i - \vec{r}_j|$. Considering the dissipative effect, the equation of the normal contact force is

$$F_{ij}^n = k_n\delta + \gamma_n v_n, \tag{14}$$

where k_n and γ_n are the spring stiffness and the dissipative coefficient, respectively, and v_n is the normal component of the relative velocity $\vec{v}_{ij} = \vec{v}_i - \vec{v}_j$. This is called Linear Spring Dashpot (LSD) model. Why do we select a linear mode other than the Hertz contact mode (a non-linear mode)? The reason is that the Hertz mode is based on an assumption that the loads applied to the particles are static [36]. The coefficient of restitution of two particles in the Hertz model is dependent on the relative velocity during colliding. When the clustering occurs in granular gas, the distribution of velocity of particles has a larger range. This will cause a larger variation of the coefficient of restitution. It's not correspondent with practice. For a dense packing system, the Hertz model is more suitable.

The tangential contact force is determined by the tangential component of the relative velocity and the normal contact force

$$F_{ij}^t = \min(\gamma_t v_{ij}^t, \mu F_{ij}^n), \tag{15}$$

where γ_t is a constant, μ is the friction coefficient and v_{ij}^t is the tangential component of $\vec{v}_{ij}$. Figure 13 shows the mechanism of the contact model in this work.

According to the LSD model, the collision process between two particles acts like a damped harmonic oscillator. We can get the contact duration t_C, half of the period of the damped harmonic oscillator, analytically,

$$t_c = \pi/\sqrt{k_n/m_{ij} - \gamma_n^2/4m_{ij}^2}, \tag{16}$$

Fig. 13 The mechanism of the contact model (adapted from Wang et al. [1])
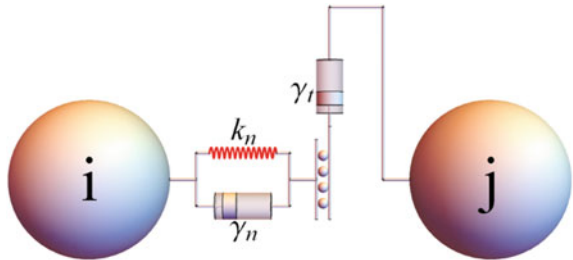
where m_{ij} is the reduced mass $m_{ij} = m_i m_j / (m_i + m_j)$. Using the oscillation half period, we obtain the coefficient of restitution by the ratio of the final velocity and the initial velocity,

$$e = v_{final}/v_0 = \exp(-\gamma_n t_c / 2m_{ij}). \tag{17}$$

By solving Eq. (17), we can get the dissipative coefficient γ_n via the restitution coefficient e,

$$\gamma_n = -2\sqrt{k_n m_{ij}} \ln(e) / \sqrt{\ln^2(e) + \pi^2}. \tag{18}$$

Using LSD model, the coefficient of restitution is a constant independent of the relative velocity of two particles during collision. Additionally, in order to guarantee the simulation's accuracy, the time duration per step Δt is required to be much less than t_C, i.e. $\Delta t \ll t_c$. In the simulation the step duration is taken as $\Delta t \approx t_C/10$.

2.2 Experimental

Figure 14a is a photo of the two-compartment sample cell used in the experiment of the recoverable satellite "SJ-10". Grains in the cell are driven by four independently moving pistons, which are used as the end walls of the two compartments as plotted in Fig. 14b. The two compartments are connected by a window of 12 mm wide. The total length of the cell is 100 mm, as seen in Fig. 14b, and the individual piston size is 25×25 mm. The four pistons are driven by two linear motors. Each motor controls either left- or right-end two pistons, so that the two pistons at the same side vibrate synchronously. The piston's position, vibration frequency and amplitude are pre-programmed. In order to prevent the electrostatic effect, metallic particles are used and the cell is made of metal and has been grounded. The fused silica window plates are coated by conductive thin films. Particles are enclosed between the left and right pistons. The volumes of the two cells can then be controlled by the positions of the pistons.

2.3 Numerical

2.3.1 Double-Cell

The numerical parameters of the granular cell system are taken same as that in the experiments shown in Fig. 14b. In the simulation, the particle radius R is 0.5 mm. The density ρ of particles is 4500 kg/m^3. The coefficient of restitution e for grain-grain collision is taken as 0.8. The coefficient of friction μ is 0.3. The total number
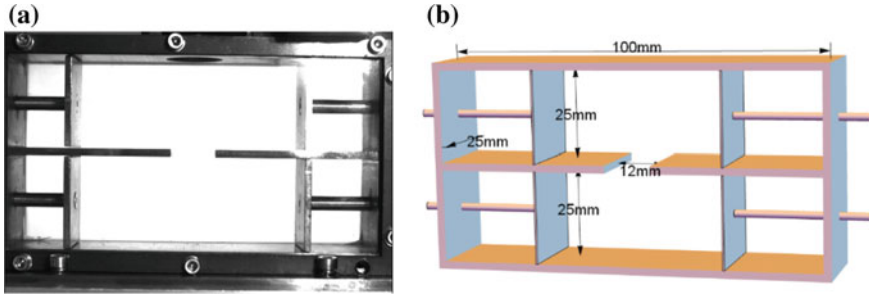
Fig. 14 **a** A photograph of the two-compartment sample cell used in the experiment of the recoverable satellite "SJ-10"; **b** Sketch of the setup (adapted from Wang et al. [1])

of particles in the connected two-compartment cell is taken as N. The number in one (say upper one) cell is N_1, and the number in the other (lower) cell is $N_2 = N - N_1$. To start with, we put particles evenly in each compartment. The initial velocity is arbitrarily set to be 0.1 m/s with random direction.

2.3.2 Single-Cell

Simulations of particles in single cell are performed to investigate in zero gravity the particle distribution along the vibration direction. With gravity, using the equation of gas state, Eggers [55] sets up a flux function to model the segregation phenomenon. In space under microgravity we need to know the profile of the particle distribution to set up a flux function in order to find the segregation condition. To know the number of particles flow instantaneously through the window per unit time, we count the number of particle-wall collisions at the virtual window of the cell [66]. The size of the single-cell is $80 \times 25 \times 25$ mm. Three rectangular shades along the side wall are shown in Fig. 15 to indicate the virtual windows at different positions. We record
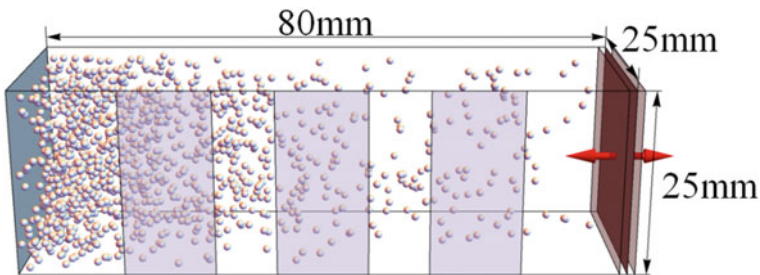

Fig. 15 Schematic of the virtual-window single cell. Particles are excited by the right-end moving wall. The virtual window at three different locations are indicated by rectangular shades at the side wall (adapted from Wang et al. [1])

how many times particles collide with a given virtual window at a time interval for a sufficiently long time. The flux profile can then be given by the counts of collisions per unit time across a given virtual window.

2.4 Results

2.4.1 Distribution of Particles in Single Cell

Under gravity in Eggers' model [55] the equation of gas state is conveniently used for the density distribution of particles along the vibration direction. In microgravity the particle distribution is determined by the geometry of the cell and the wall excitation condition. We, therefore, perform a numerical study in a same cell geometry configuration and wall excitation condition to obtain the zero-gravity particle distribution. One set of the simulation results at condition that frequency $f_r = 10$ Hz and shaking amplitude $A_r = 3$ mm, is shown in Fig. 16. Dividing the cell into 20 equal parts along the vibration direction, particle counts in each division are averaged for different total number N. Except for situation in Fig. 16a when $N = 500$, particle distributions in steady state for N greater than 1000 show exponential distribution along x-axis, which means similar distribution as the situation with gravity is achievable. For N is less than 1000, the distribution is relatively homogeneous. With greater number N, particles gather denser to the cool end. When the number N is 2000, nearly 40% of particles cluster in 5% of the total volume.
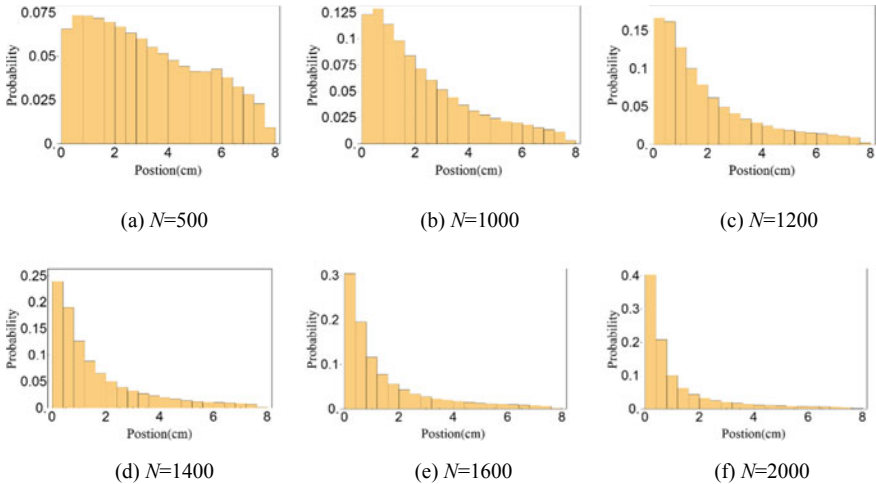

Fig. 16 Density distribution of particles in single cell with different numbers of particles (adapted from Wang et al. [1])

2.4.2 Flux Function Obtained in Virtual-Window Single-Cell Simulation

Finding flux function is necessary to understand the occurrence of the segregation. The segregation is governed by the following equation:

$$\frac{dN_i(t)}{dt} = -F(N_i(t)) + F(N - N_i(t)), \quad i = 1, 2, \tag{19}$$

where the $N_1(t)$ and $N_2(t)$ are the counts of particles in the two compartments at time t, and $F(N_i)$ is the number of particles per unit time at time t that flow from a compartment containing N_i particles to another compartment. Once knowing the function $F(N_i)$, $N_i(t)$ can be obtained from Eq. (19).

In order to characterize the segregation of particles in the two cells, a dimensionless parameter ε_i is introduced:

$$\varepsilon_i = (N_i - N/2)/N, \quad i = 1, 2. \tag{20}$$

Figure 17 shows a plot of simulation result how ε_i changes with time. It takes some time for the population $N_i(t)$ to reach a steady state. We call this time as the waiting time τ. At any time $\varepsilon_1(t) = -\varepsilon_2(t)$, and the absolute value of ε_i at the steady state is indicated as ε. $\varepsilon = 0$ means particles are equally populated in the two cells, and $|\varepsilon| = 0.5$ means all the particles gather in one compartment, i.e., fully segregated.

The flux function obtained by the virtual-window single-cell simulation method [66] is shown in Fig. 18a for three locations of the window. A non-monotonic function $F(N_i)$ guaranteed the occurrence of the segregation. A weakly position dependence of the flux function shown in Fig. 18a tells us that flux value is greater when the window position is moving away from the moving wall. Numerically solving the Eq. (19), from $N_i(t)$ we get the value $|\varepsilon_i(t)|$ and compare it with the simulation results, as shown in Fig. 18b. The comparison is qualitatively well except the time

Fig. 17 One example of simulation result of $\varepsilon_i(t)$ (adapted from Wang et al. [1])
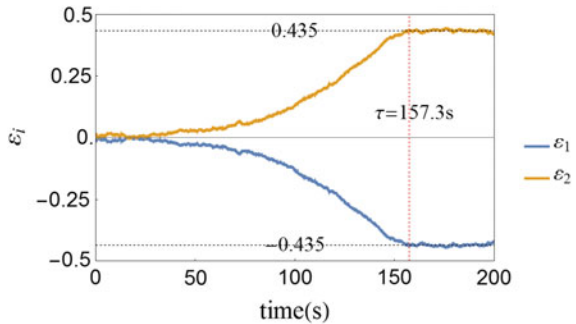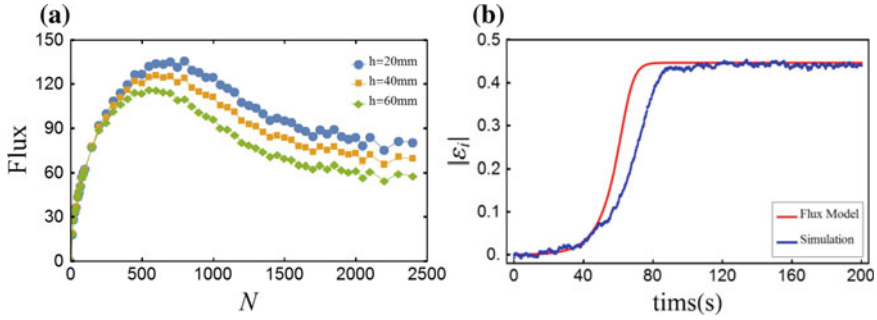
Fig. 18 **a** Flux as a function of the number N; **b** Comparison between the theoretical result from the flux model and the simulation result (adapted from Wang et al. [1])

during 60–80 s. The flux mode describes the process of the segregation in granular gas theoretically. But in numerical simulation or experiment, the fluctuation in the granular system may promote or delay the occurrence of Maxwell's demon.

2.4.3   The Effect of Total Number N on the Segregation ε

In the SJ-10 experiment, the segregation is observed at total particle number $N = 2400$, cell length $= 80$ mm, and with right-end shaking at frequency $f = 7$ Hz, amplitude $A = 2$ mm, (equivalently acceleration $\Gamma = 0.38g$). The vibration intensity is characterized by the acceleration $\Gamma = A_r (2\pi f_r)^2/g$, where g is the acceleration of gravity. In the simulation, we set amplitude A to be fixed and change frequency of the right piston to change the shaking acceleration Γ. Figure 19a–d are snapshots captured in the experiment at four different times. It shows the distribution segregation is fully developed at the time $t = 176$ s.

Using similar parameters, a simulation is performed and a comparison shows consistent results as seen in Fig. 19e–h. Initially particles are distributed equally in

(a) t=0s   (b) t=48s   (c) t=96s   (d) t=176s

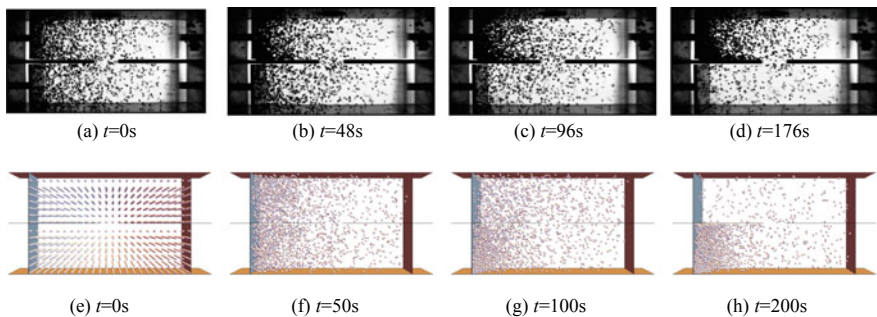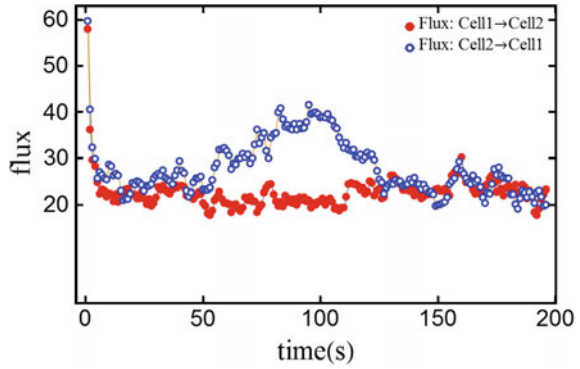(e) t=0s   (f) t=50s   (g) t=100s   (h) t=200s

Fig. 19 **a–d** Snapshots captured in the experiments at different time; **e–h** Snapshots in the simulations taken at similar time (adapted from Wang et al. [1])

Fig. 20 Flux as a function of time (adapted from Wang et al. [1])

the two cells. Segregation appears after about 100 s, and is fully developed 200 s afterwards.

Figure 20 shows the dependence of the flux, i.e. the counts per unit time of particles flowing from one cell to the other, on time. The red (blue) dots in Fig. 20 show the flux from cell 1(2) to cell 2(1) along time. In the initial few seconds, the flow rates from cell 1(2) to cell 2(1) are quickly decreasing at about the same speed. Numbers of particles in two cells are almost equal, and the flux from one cell to the other is nearly equal to the flux of the opposite direction, namely the net flux is nearly zero. At some instant if cell 2 happens to have more particles flowing out than flowing in, less particles will be in cell 2 and less inelastic collisions will cause particles in cell 2 move faster on average than particles in cell 1. There will be a positive feedback to induce even more particles flow out from cell 2 to cell 1 until most of the particles are in cell 1 and almost no more particles can flow from cell 2 to cell 1. At this time the flux from either cell will be the same again, and the net flux will be zero again.

Next, we take the advantage of computer simulation to study the effect of total number of particles in the segregation conditions under no gravity.

Next we change the total number N from 800 to 1500. Figure 21a gives us the results how $\varepsilon_i(t)$ changes with N. When the total number N is less than or equal to 1100, the asymmetry ε fluctuate around 0. Segregation does not occur. Only when N exceeds a critical value (here the critical value is about 1100) the segregation occurs. Figure 21b shows that the asymmetry parameter ε grows from 0 and approaches 0.5 with increasing N.

2.4.4 Effect of Excitation Acceleration on the Segregation

Figure 22a gives the simulation results of the asymmetry parameter $|\varepsilon_i|$ changing with time under different Γ. For higher acceleration Γ, $|\varepsilon_i|$ reaches steady state value ε faster.

Since in microgravity experiments the operational time is normally limited, the waiting time τ is important to know in advance, which tells us how long to wait for seeing the effect. As shown in Fig. 22b, the rate $1/\tau$ seems linearly proportional to
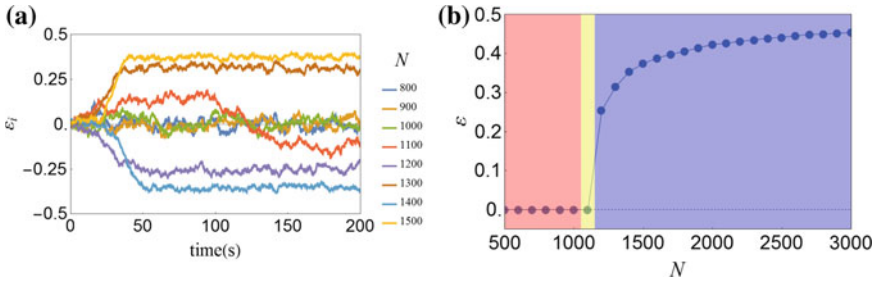
Fig. 21 **a** Variation of the asymmetry parameters ε under different N as a function of time; **b** Variation of the asymmetry parameter ε in the steady state as a function of N (adapted from Wang et al. [1])
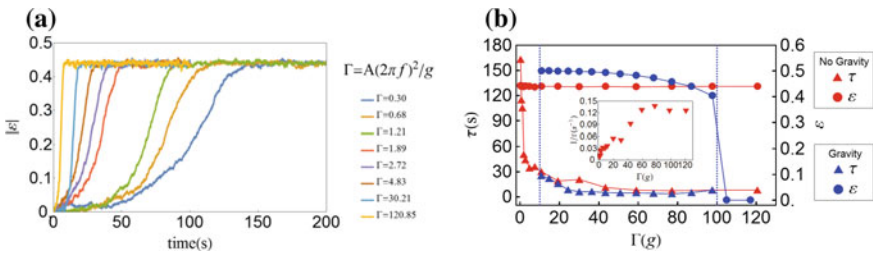

Fig. 22 **a** The asymmetry parameter $|\varepsilon|$ reaches the steady state after waiting time τ; **b** Effects of the vibration intensity on the asymmetry parameter ε and the waiting time τ under gravity and no gravity (adapted from Wang et al. [1])

Γ at low Γ. Only when Γ is high enough the rate $1/\tau$ reaches a maximum value. For the Γ value available in our microgravity experiment (normally less than 1 g), Fig. 22b tells us the time duration τ shall be of the order of 100 s. This result helps us in determining the experimental design.

In Fig. 22b, it shows that the waiting time τ does not go to zero, there is a minimum time required for particles to go to the steady segregation state no matter how strong the vibration intensity goes. In our case the value is of the order of 10 s.

The above numerical results are quite different with the experiments in gravity. With gravity particles act like gas molecules, and distribute in both cells. No segregation of the granular gas is observed at high Γ when particle random collisions dominate. When Γ is below a certain threshold, no segregation is observed either as the gravitational force dominates. With no gravity, the segregation ε becomes a constant and does not depend on Γ, as seen in Fig. 22b, but the waiting time τ depends strongly on Γ.

2.4.5 Effect of the Position of the Opening on the Segregation

The effect of the window position is investigated by changing the piston location. We change the length (volume) of the cell and the distance of the window from

either side of the pistons. The window connecting the two compartments is located at a position x_l from the position of the left piston. The right piston is accelerated at 4.83 g (where $f_r = 20$ Hz and $A_r = 3$ mm). The effects on both the waiting time τ and the asymmetry parameter ε are shown in Fig. 23. The segregation efficiency is better when the window is closer to the cool-end window. As is shown in Fig. 23b, the value of ε changes from 0.44 to 0.36 when x_l changes from 10 to 35 mm. It means the segregation is more efficient when the window is closer to the cool-end. However, to reach the steady segregation we need to wait longer time when the window is closer to the cool-end as the time τ increases, as is seen in Fig. 23b.

The previous researches show that the window's position has influence on the occurrence of the segregation under gravity, namely that only when the window's position is closer enough to the bottom, the segregation can appear. Our numerical results in Fig. 24 also show the same result. When gravity does not play a role, the position effect to the segregation becomes weaker.

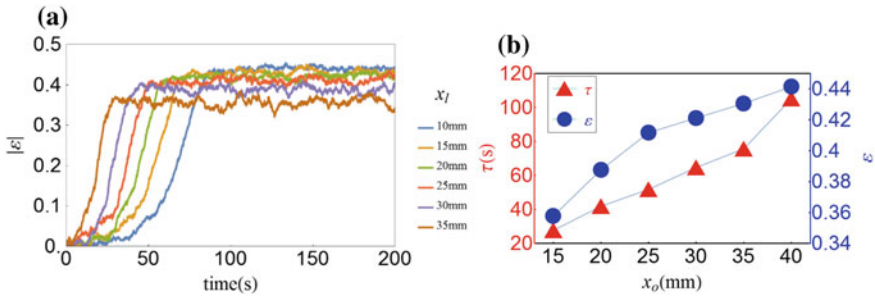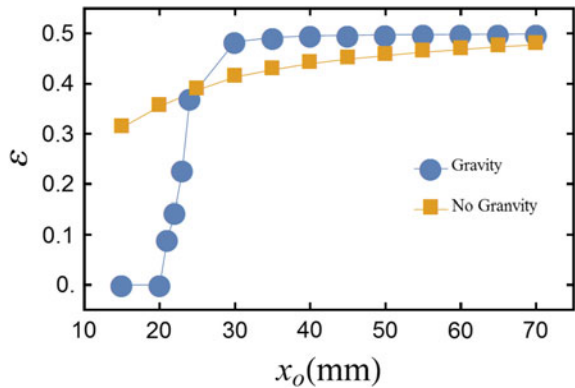**Fig. 23 a** Variation of the asymmetry parameter $|\varepsilon_i|$ as a function of time; **b** The waiting time τ (red triangular dots) and the asymmetry parameter ε (blue dots) as a function of window position (adapted from Wang et al. [1])

Fig. 24 The asymmetry parameter ε as a function of opening position with and without gravity (adapted from Wang et al. [1])

3 Summary

The microgravity-experimental and simulation results on the granular gas freely cooling process support Haff's law that the kinetic energy dissipates with time t as $E(t) \sim (1 + t/\tau)^{-2}$. The effects of particle number density and the particle size on τ, due to the rotation and friction during collision, are studied in simulation. A modified τ is given to take into account the dissipation due to frictions. The collision frequency affected by the number density and particle size is discussed. From the standard deviation of the velocity distribution we also verify the energy dissipation law, showing its good consistence with the Haff's Kinetic energy dissipation.

The investigation in two-connected-cells clustering shows granular segregation is achievable at zero gravity with a different condition from the case under gravity. With gravity, the segregation depends on Γ and can be divided into three regimes: one at low Γ when the gravitational force is dominant that no segregation appears and ε is zero; a second regime when Γ is at an intermediate value that segregation appears and ε becomes non-zero; and the third regime when Γ is high enough that random particle collisions dominate and ε becomes zero again. Under zero gravity, segregation ε does not depend on Γ. It is a constant weakly dependent on the position of the window. A minimum excitation time is necessary to observe the phenomenon with or without gravity. This time τ, however, depends strongly on the value Γ. With the affordable acceleration Γ in satellite condition, the excitation time is on the order of a few minutes, which means no segregation can be seen in drop tower or parabolic experiments [90] which offer microgravity condition only for a short time (3–22 s).

References

1. Wang W, Zhou Z, Zong J, Hou M (2017) Dem simulation of granular segregation in two-compartment system under zero gravity. Chin Phys B 26:044501
2. Wang W, Hou M, Chen K, Yu P, Sperl M (2018) Experimental and numerical study on energy dissipation in freely cooling granular gases under microgravity. Chin Phys B 27:084501
3. Jaeger HM, Nagel SR, Behringer RP (1996) Granular solids, liquids, and gases. Rev Mod Phys 68:1259
4. De Gennes PG (1999) Granular matter: a tentative view. Rev Mod Phys 71:S374
5. Kadanoff LP (1999) Built upon sand: theoretical ideas inspired by granular flows. Rev Mod Phys 71:435
6. Goldhirsch II, Zanetti G (1993) Clustering instability in dissipative gases. Phys Rev Lett 70:1619
7. McNamara S, Young WR (1994) Inelastic collapse in two dimensions. Phys Rev E 50:R28
8. Falcon É, Wunenburger R, Évesque P, Fauve S, Chabot C, Garrabos Y, Beysens D (1999) Cluster formation in a granular medium fluidized by vibrations in low gravity. Phys Rev Lett 83:440
9. Luding S, Herrmann HJ (1999) Cluster-growth in freely cooling granular media. Chaos 9:673
10. Painter B, Dutt M, Behringer RP (2003) Energy dissipation and clustering for a cooling granular material on a substrate. Phys D 175:43
11. Miller S, Luding S (2004) Cluster growth in two- and three-dimensional granular gases. Phys Rev E 69:031305

12. Efrati E, Livne E, Meerson B (2005) Hydrodynamic singularities and clustering in a freely cooling inelastic gas. Phys Rev Lett 94:088001
13. Meerson B, Puglisi A (2005) Towards a continuum theory of clustering in a freely cooling inelastic gas. Europhys Lett 70:478
14. Aranson IS, Tsimring LS (2006) Patterns and collective behavior in granular media: theoretical concepts. Rev Mod Phys 78:641
15. Fingerle A, Herminghaus S (2006) Unclustering transition in freely cooling wet granular matter. Phys Rev Lett 97:078001
16. Yu P, Frank-Richter S, Börngen A, Sperl M (2014) Monitoring three-dimensional packings in microgravity. Granul Matter 16:165
17. Chen Y, Pierre E, Hou M (2012) Breakdown of energy equipartition in vibro-fluidized granular media in micro-gravity. Chin Phys Lett 29:074501
18. Mei Y, Chen Y, Wang W, Hou M (2016) Experimental and numerical study on energy dissipation in freely cooling granular gases under microgravity. Chin Phys B 25:084501
19. Wang Y (2017) Granular packing as model glass formers. Chin Phys B 26:014503
20. Haff PK (1983) Grain flow as a fluid-mechanical phenomenon. J Fluid Mech 134:401
21. Brito R, Ernst MH (1998) Extension of Haff's cooling law in granular flows. Europhys Lett 43:497
22. Luding S, Huthmann M, McNamara S, Zippelius A (1998) Zippelius, homogeneous cooling of rough, dissipative particles: theory and simulations. Phys Rev E 58:3416
23. Garzó V, Dufty J (1999) Homogeneous cooling state for a granular mixture. Phys Rev E 60:5706
24. Huthmann M, Orza JAG, Brito R (2000) Dynamics of deviations from the gaussian state in a freely cooling homogeneous system of smooth inelastic particles. Granul Matter 2:189
25. Zaburdaev VY, Brinkmann M, Herminghaus S (2006) Free cooling of the one-dimensional wet granular gas. Phys Rev Lett 97:018001
26. Hayakawa H, Otsuki M (2007) Long-time tails in freely cooling granular gases. Phys Rev E 76:051304
27. Meerson B, Fouxon I, Vilenkin A (2008) Nonlinear theory of nonstationary low mach number channel flows of freely cooling nearly elastic granular gases. Phys Rev E 77:021307
28. Santos A, Montanero JM (2009) The second and third sonine coefficients of a freely cooling granular gas revisited. Granul Matter 11:157
29. Kolvin I, Livne E, Meerson B (2010) Navier-Stokes hydrodynamics of thermal collapse in a freely cooling granular gas. Phys Rev E 82:021302
30. Mitrano PP, Garzo V, Hilger AM, Ewasko CJ, Hrenya CM (2012) Assessing a hydrodynamic description for instabilities in highly dissipative, freely cooling granular gases. Phys Rev E 85:041303
31. Brilliantov NV, Pöschel T (2000) Velocity distribution in granular gases of viscoelastic particles. Phys Rev E 61:5573
32. McNamara S, Luding S (1998) Energy nonequipartition in systems of inelastic, rough spheres. Phys Rev E 58:2247
33. Ben-Naim E, Chen SY, Doolen GD, Redner S (1999) Shock like dynamics of inelastic gases. Phys Rev Lett 83:4069
34. Nie X, Ben-Naim E, Chen S (2002) Dynamics of freely cooling granular gases. Phys Rev Lett 89:204301
35. van Zon JS, MacKintosh FC (2004) Velocity distributions in dissipative granular gases. Phys Rev Lett 93:038001
36. Shinde M, Das D, Rajesh R (2007) Violation of the porod law in a freely cooling granular gas in one dimension. Phys Rev Lett 99:234505
37. Shinde M, Das D, Rajesh R (2009) Equivalence of the freely cooling granular gas to the sticky gas. Phys Rev E 79:021303
38. Shinde M, Das D, Rajesh R (2011) Coarse-grained dynamics of the freely cooling granular gas in one dimension. Phys Rev E 84:031310
39. Villemot F, Talbot J (2012) Homogeneous cooling of hard ellipsoids. Granul Matter 14:91

40. Pathak SN, Das D, Rajesh R (2014) Inhomogeneous cooling of the rough granular gas in two dimensions. Europhys Lett 107:44001
41. Pathak SN, Jabeen Z, Das D, Rajesh R (2014) Energy decay in three-dimensional freely cooling granular gas. Phys Rev Lett 112:038001
42. Maaß CC, Isert N, Maret G, Aegerter CM (2008) Experimental investigation of the freely cooling granular gas. Phys Rev Lett 100:248001
43. Tatsumi S, Murayama Y, Hayakawa H, Sano M (2009) Experimental study on the kinetics of granular gases under microgravity. J Fluid Mech 641:521
44. Burton JC, Lu PY, Nagel SR (2013) Energy loss at propagating jamming fronts in granular gas clusters. Phys Rev Lett 111:188001
45. Harth K, Trittel T, Wegner S, Stannarius R (2018) Competitive clustering in a bidisperse granular gas. Phys Rev Lett 120:214301
46. Berry MV, Geim AK (1997) Of flying frogs and levitrons. Eur J Phys 18:307
47. Luding S (2008) Cohesive, frictional powders: contact models for tension. Granul Matter 10:235
48. Opsomer E, Ludewig F, Vandewalle N (2012) Dynamical clustering in driven granular gas. Europhys Lett 99:40001
49. Clément E, Duran J, Rajchenbach J (1992) Experimental study of heaping in a two-dimensional sand pile. Phys Rev Lett 69
50. Jia LC, Lai PY, Chan CK (1999) Empty Site models for heap formation in vertically vibrating grains. Phys Rev Lett 83:3832
51. Lai PY, Jia LC, Chan CK (2000) Symmetric heaping in grains: a phenomenological model. Phys Rev E 61:5593
52. Hong DC, Quinn PV, Luding S (2001) Reverse Brazil nut problem: competition between percolation and condensation. Phys Rev Lett 86:3423
53. Breu APJ, Ensner HM, Kruelle CA, Rehberg I (2003) Reversing the Brazil-Nut effect: competition between percolation and condensation. Phys Rev Lett 90:014302
54. Schlichting HJ, Nordmeier V (1996) Math. Naturwiss. Unterr. 49323 (in German)
55. Eggers J (1999) Sand as Maxwell's Demon. Phys Rev Lett 83:5322
56. van der Weele K, van der Meer D, Versluis M, Lohse D (2001) Hysteretic clustering in granular gas. Europhys Lett 53:328
57. van der Meer D, Reimann P, van der Weele K, Lohse D (2004) Spontaneous ratchet effect in a granular gas. Phys Rev Lett 92:184301
58. van der Meer D, van der Weele K, Lohse D (2001) Bifurcation diagram for compartmentalized granular gases. Phys Rev E 63:061304
59. Meerson B, Pöschel T, Sasorov PV, Schwager T (2004) Giant fluctuations at a granular phase separation threshold. Phys Rev E 69:021302
60. Costantini G, Paolotti D, Cattubo C, Marconi UMB (2005) Bistable clustering in driven granular mixtures. Phys A 347:411–428
61. Lambiotte R, Salazar JM, Brenig L (2005) From particle segregation to the granular clock. Phys Lett A 343:224–230
62. Liu R, Li Y, Hou M (2007) Van der Waals-like phase-separation instability of a driven granular gas in three dimensions. Phys Rev E 75:061304
63. Liu R, Li Y, Hou M (2009) Oscillatory phenomena of compartmentalized bidisperse granular gases. Phys Rev E 79:052301
64. Hou M, Li Y, Liu R, Zhang Y, Lu K (2010) Oscillatory clusterings in compartmentalized granular systems. Phys Status Solidi A 207:2739–2749
65. Li Y, Hou M, Evesque P (2011) Directed clustering in driven compartmentalized granular gas systems in zero gravity. J Phys: Conf Ser 327:012034
66. Li Y, Liu R, Shinde M, Hou M (2012) Flux measurement in compartmentalized mono-disperse and bi-disperse granular gases. Granular Matter 14:137–143
67. Li Y, Liu R, Hou M (2012) Gluing bifurcation and noise-induced hopping in the oscillatory phenomena of compartmentalized bidisperse granular gases. Phys Rev Lett 109:198001

68. Shah SH, Li Y, Cui F, Evesque P, Hou M (2012) Irregular oscillation of bi-disperse granular gas in cyclic three compartments. Chin Phys Lett 29:034501
69. Bray JJ, Moreno F, García-Rojo R, Ruiz-Montero MJ (2001) Hydrodynamic Maxwell Demon in granular systems. Phys Rev E 65:011305
70. Lipowski A, Droz M (2002) Urn model of separation of sand. Phys Rev E 65:031307
71. Marconi UMB, Conti M (2004) Dynamics of vibrofluidized granular gases in periodic structures. Phys Rev E 69:011302
72. Mikkelsen R, van der Meer D, van der Weele K, Lohse D (2004) Competitive clustering in a bidisperse granular gas: experiment, molecular dynamics, and flux model. Phys Rev E 70:061307
73. Leconte M, Evesque P (2006) Maxwell demon in granular gas: a new kind of bifurcation? The hypercritical bifurcation. Physics 0609204
74. Lai P, Hou M, Chan C (2009) Granular gases in compartmentalized systems. J Phys Soc Jpn 78:041001
75. Mikkelsen R, van der Meer D, van der Weele K, Lohse D (2002) Competitive clustering in a bidisperse granular gas. Phys Rev Lett 89:214301
76. van der Meer D, van der Weele K, Lohse D (2002) Sudden collapse of a granular cluster. Phys Rev Lett 88:174302
77. Jean P, Bellenger H, Burban P, Ponson L, Evesque P (2002) Phase transition or Maxwell's Demon in granular gas. Pourders Grains 13:27–39
78. Mikkelsen R, van der Weele K, van der Meer D, van Hecke M, Lohse D (2005) Small-number statistics near the clustering transition in a compartmentalized granular gas. Phys Rev E 71:041302
79. Miao T, Liu Y, Miao F, Mu Q (2005) On cyclic oscillation in granular gas. Chin Sci Bull 50:726–730
80. Viridi S, Schmick M, Markus M (2006) Experimental observations of oscillations and segregation in a binary granular mixture. Phys Rev E 74:04130
81. Hou M, Tu H, Liu R, Li Y, Lu K (2008) Temperature oscillations in a compartmentalized bidisperse granular gas. Phys Rev Lett 100:068001
82. Hou M, Liu R, Zhai G, Sun Z, Lu K, Garrabos Y, Evesque P (2008) Velocity distribution of vibration-driven granular gas in knudsen regime in microgravity. Microgravity Sci Technol 20:73–80
83. Isert N, Maaß CC, Aegerter CM (2009) Influence of gravity on a granular Maxwell's Demon experiment. Eur Phys J E 28:205–210
84. Shah SH, Li Y, Cui F, Hou M (2012) Directed segregation in compartmentalized bi-disperse granular gas. Chin Phys B 21:014501
85. Zhang Y, Li Y, Liu R, Cui F, Evesque P, Hou M (2013) Imperfect pitchfork bifurcation in asymmetric two-compartment granular gas. Chin Phys B 22:054701
86. Opsomer E, Noirhomme M, Vandewalle N, Ludewig F (2013) How dynamical clustering triggers Maxwell's Demon in microgravity. Phys Rev E 88:012202
87. Noirhomme M, Opsomer E, Vandewalle N, Ludewig F (2015) Granular transport in driven granular gas. Eur Phys J E38
88. Luding S (2008) Cohesive, frictional powders: contact models for tension. Granular Matter 10:235–246
89. Dintwa E, Tijskens E, Ramon H (2007) On the accuracy of the hertz model to describe the normal contact of soft elastic spheres. Granular Matter 10:209–221
90. Wang H, Chen Q, Wang WG, Hou MY (2016) Experimental study of clustering behaviors in granular gases. Acta Phys Sin 65:014502